Computers and Electronics in Agriculture 99 (2013) 124–131

Contents lists available at ScienceDirect

Computers and Electronics in Agriculture

journal homepage: www.elsevier.com/locate/compag

Time-optimal guidance control for an agricultural robot with orientation constraints

Fuhong Dong *, Olaf Petzold, Wolfgang Heinemann, Roland Kasper

Institute of Mobile Systems (IMS), Faculty of Mechanical Engineering, Otto-von-Guericke University Magdeburg, Universitätsplatz 2, D-39106 Magdeburg, Germany

ARTICLE INFO

Article history:
Received 3 February 2013
Received in revised form 13 September 2013
Accepted 14 September 2013

Keywords:
Field robot
Automatic guidance
Time-optimal control
Cascade control
Differential drive

ABSTRACT

This paper deals with time-optimal control for the row guidance system of an autonomous field robot with differential drive. The movement of the robot is concretely constrained by the plant cultivation environment. A time-optimal differential velocity profile is generated based on optimal control theory to eliminate any initial error or tracking deviation. To allow for an efficient implementation on a micro-processor, a substitute controller is suggested to perform the minimum-time guidance task. The substitute with a cascade structure is proposed using PID algorithms. The computational efficiency is consequently improved and the system is more convenient to be carried out on a micro-processor. The performance of the proposed substitute system is investigated through numerical studies by comparison with the time-optimal controller. Experiments are comprehensively conducted indoors and outdoors to evaluate the proposed row guidance regime. The results show the satisfactory performance and efficiency with a high precision of ±3 cm in the field.

1. Introduction

In the past decades, autonomous agricultural machinery has been subjected to extensive studies due to labor shortage, food product quality and safety, as well as the environmental impact. Automatic harvesting machines were extensively studied for cucumber (Van Henten et al., 2003), cherry (Tanigaki et al., 2008) and white asparagus (Chatzimichali et al., 2009). Special autonomous robots were also suggested for greenhouse applications by Mehta et al. (2008) and Sànchez-Hermosilla et al. (2010). A number of researchers actively investigated automatic machines for weeding control based on machine vision and Real-time Kinematic Global Positioning Systems (RTK GPS). Considerable efforts have been made by Straten's group based on machine-vision and RTK GPS system in weeding control for sugar beet (Bakker et al., 2004, 2011). The main techniques for weeding control were thoroughly summarized by Slaughter et al. (2008). Autonomous differential-drive wheeled mobile robots are able to track almost all the possible desired paths, and have been widely used in well structured environment such as factories, warehouses and offices (Díaz del Río et al., 2001; Feng et al., 1993; Gracia and Tornero, 2008). In agricultural applications, differential-drive wheeled mobile robots have been also applied as platform or chassis to carry the associate apparatus like harvesting robot arm or spraying pistol for weeds (Åstrand and Baerveldt, 2002; Mehta et al., 2008; Van Henten et al., 2003; Xue et al., 2012). An automated row guidance control system is necessary for the autonomous agricultural robots to operate within rowed crops collision-freely to perform various tasks. Differently from the well-structured environment, the working environment of agricultural robots imposes varied constraints on the movements of the vehicles due to contact surface of loose soil and the specialties of crop cultivation features. The row guidance system of the autonomous agricultural robots is expected to be:

- Feasible: efficient and easy to be put into practice,
- Safe: avoiding dangerous motions and collisions with crops,
- High precision tracking: to operate safely within limited working space between rows,
- Low computational costs: to perform the real-time following algorithms on a single chip.

In this work we focus on the development and implementation of the time-optimal row guidance system of an autonomous field robot. The field mobile robot was developed as a platform for white asparagus harvesting. In contrast to the most often reported technologies in row identification based on machine-vision and RTK GPS which were summarized by Slaughter et al. (2008), the position of the target row for this robot is detected using sonar sensors benefiting from the erected cultivation bed. The up-erected cultivation bed of white asparagus provides a natural surface for the sonar sensors. This design not only relieves the computation effort

* Corresponding author. Tel.: +49 391 67 51712; fax: +49 391 67 12656.
E-mail address: fuhong.dong@ovgu.de (F. Dong).

0168-1699/$ - see front matter © 2013 Elsevier B.V. All rights reserved.
http://dx.doi.org/10.1016/j.compag.2013.09.009

of the processor in comparison with the machine-vision based application, but also reduces the investment. The study of this work is done based on our previous research (Dong et al., 2011). In that paper, a row guidance system based on conventional PID method was suggested for the prior try. The row following performance was verified in labor. However, since the robot movement is closely constrained by its working environment, the initial error and following deviation are expected to be eliminated as quickly as possible to achieve a stable operation. In this paper, we investigate firstly the simulation study of the time-optimal control problem of the row guidance system. Due to the very limited investment in the machine's cost, the realization of the time-optimal control is not feasible on a current micro-processor. Finally, we realize the guidance performance of the time-optimal control using a practical substitute system by improving the previous row guidance controller based on PID algorithms. The row following performance of the substitute system is extensively evaluated through comparison with the results of time-optimal control system in simulation studies, and further investigated experimentally in laboratory as well as in the field.

The outline of this paper is arranged as follows. The mechanical design of the harvesting robot platform is described in the following Section 2. In Section 3 the kinematic model of the robot and the environmental constraints are introduced. Section 4 is devoted to formulation of minimum time problem and controller development. Section 5 firstly details the establishment of the practical substitute system for time-optimal guidance control, and then illustrates the outcome of simulation and experimental tests. The concluding remarks and future work are given in Section 6.

2. Mechanical design

The agricultural wheeled mobile robot in this work is designed as a development platform of an autonomous field machine for white asparagus harvesting. White asparagus is cultivated in parallel trapezoidal beds that are heaped up about 60 cm over ground surface. The cultivation beds are built with 80 cm intervals and 100 cm wide at the bottom. The heaped beds are always covered with a film to keep the soil moisture in order to guarantee the product's quality. The field robot is demanded to operate by striding one bed at a time. It is also necessary for the robot to have sufficient place for the harvested white asparagus spears for future development. The platform is designed for both efficiency and cost effectiveness. The dimensions of the robot base is $310 \times 180 \times 160$ cm ($l/w/h$). The platform frame has a hollow space room of $310 \times 160 \times 73$ cm ($l/w/h$) under the machine. It has a weight of 450 kg with a maximal load capacity of 200 kg. The vehicle has a rolling system to guarantee mobility and maneuverability in an environment with considerable disturbance. The platform has two drive wheels at the front with a radius of 30 cm, which are independently actuated by two DC motors, and two casters with a radius of 15 cm at the rear. The maximal velocity of the vehicle is expected 50 cm/s by considering the upcoming development of harvesting function. A 450W DC motor (MY1020Z2, Zhejiang Unite Electric Motor Co., Ltd., China) was selected under the assumption that the vehicle travels on a sandy surface with a maximal slope of 5°. Sabertooth motor driver (2×50 HV) is applied to actuate both motors. The drive wheel is connected with the DC motor axis through a second-order chain gears with a ratio of 16:1 to improve the drive force and reduce the revolution speed. Steering is accomplished only by adjusting the differential velocities of the front drive wheels. Two rechargeable batteries ($12V38AH$) supply power. The identification of the actual position of the mobile robot is absolutely essential for the autonomous operation. By utilizing the features of the cultivation bed, two ultrasonic sensors (Parallax PING))) with an angular aperture of 43° are applied to measure the front and rear side distances between robot and the target bed. The sensors are installed at the right side and vertically to the side surface of the cultivation bed, one of which is near the front drive wheel and the other near the rear. The revolution of the drive motor is sensed using an incremental optical encoder (Model 120E) with a resolution of 128 pulses per revolution. The signals of the sensors are processed by a PSoC CY8C55 processor on PSoC development board (CY8CKIT-001, Cypress Semiconductor Corporation, USA).

3. Mathematic model and environmental constraints

3.1. Kinematics

The platform of the differential drive agricultural robot is assumed to consist of rigid bodies and to move on a planar surface. The location of the robot (x,y) is represented by the center point P of the front axle in the initial coordinate system. θ is the orientation of the field robot. If the robot operates over a curvature path with an instantaneous angular speed ω, the velocities of the drive wheels v_L and v_R are given by:

$$v_L = v - \frac{L_b}{2}\omega \tag{1}$$

$$v_R = v + \frac{L_b}{2}\omega \tag{2}$$

where L_b denotes the base distance of the drive wheels, v the forward velocity of the robot at the point P. It is also assumed that the wheels are non-deformable and there is no slip between wheels and ground. The movement of the machine subjects to the non-integrable constraint

$$-\dot{x}\sin\theta + \dot{y}\cos\theta = 0 \tag{3}$$

In the initial coordinate system, the kinematic model of the field mobile robot is stated as:

$$\begin{pmatrix} \dot{x} \\ \dot{y} \\ \dot{\theta} \end{pmatrix} = \begin{pmatrix} cos\theta & 0 \\ sin\theta & 0 \\ 0 & 1 \end{pmatrix} \begin{pmatrix} v \\ \omega \end{pmatrix} \tag{4}$$

3.2. Environmental constraints

The machine is demanded to drive by striding one row at a time (see Fig. 1). The interval space ($S_B = 80$ cm) between cultivation beds limits the robot movement on both lateral offset and orientation angle. The location of the robot with respect to its target row is supervised by the front and rear side distances denoted by S_f and S_r measured by the installed ultrasonic sensors SF and SR (shown in Fig. 1(a). Because of the symmetry of the spatial arrangement, only side distances on one side are essentially sensed. For the row guidance control, the robot is only permitted to drive forward. The desired location of the robot is set to $y = 0$ and $\theta = 0$. Therefore, under conditions:

–harvesting robot 180 cm wide,
–cultivation bed 100 cm wide at the bottom,
–interval space between beds 80 cm,
–free space between wheels is 160 cm wide,
–swivel radius of rear casters is 15 cm.

The reference side distance is set $S_{ref} = 30$ cm with a sufficient margin for rear casters. The rest free region for the robot in lateral direction is $S_{ref} \pm 15$ cm. Since the robot is only permitted to drive forward, it cannot proceed with some special initial positions like $S_f^{ub} = 45$ cm and $S_r^{ub} = 45$ cm or $S_f^{lb} = 15$ cm and $S_r^{lb} = 15$ cm. These

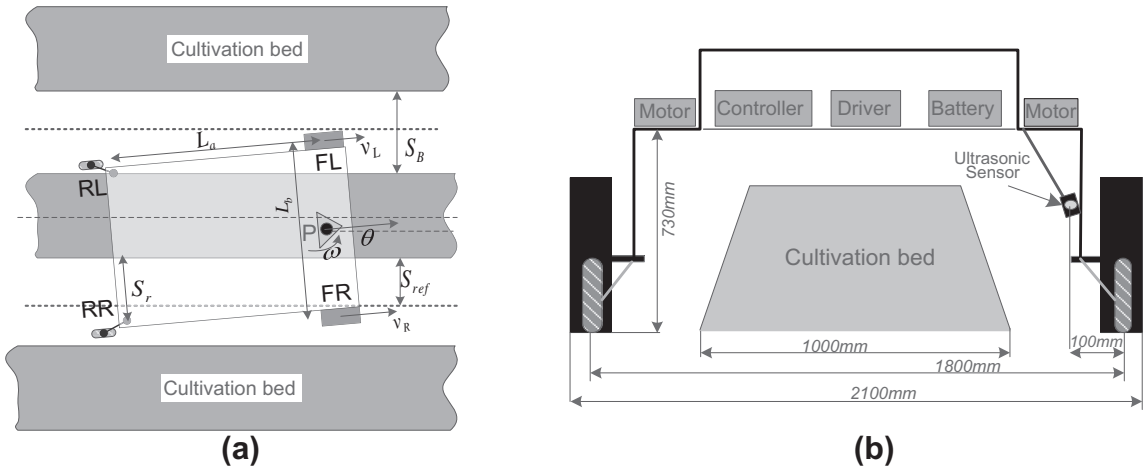

Fig. 1. Description of the robot position with respect to cultivation beds in field ((a) top view (b) side view).

situations are excluded by shrinking the permitted region of S_f by 5 cm. In conclusion, the constraints on S_f and S_r are:

$$20\text{ cm} \leqslant S_f \leqslant 40\text{ cm} \tag{5}$$

$$15\text{ cm} \leqslant S_r \leqslant 45\text{ cm} \tag{6}$$

4. Time-optimal control of row guidance system

The state equations of dynamics model are formulated based on the kinematics of the differential-drive mobile machine. The aim of the time-optimal row guidance control is to find a control law that minimizes the converging time.

4.1. Problem formulation of guidance time-optimal control

In the robot moving frame shown in Fig. 2, the positions of the front and rear ultrasonic sensors are described by vector $\mathbf{r}_f$ and $\mathbf{r}_r$ as follows:

$$\mathbf{r}_f = \begin{pmatrix} 0 \\ -\frac{L_b}{2} \\ 0 \end{pmatrix} \quad \mathbf{r}_r = \begin{pmatrix} -L_a \\ -\frac{L_b}{2} \\ 0 \end{pmatrix} \tag{7}$$

where L_a is the length of the robot platform. With help of the transformation matrix T from the moving frame to the initial frame, the linear velocity vector $\mathbf{v}$ and angular speed vector $\boldsymbol{\Omega}$:

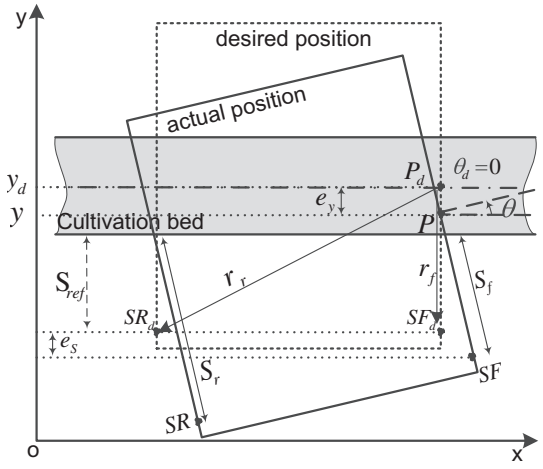

Fig. 2. Graphic representation of the guidance deviation.

$$T = \begin{pmatrix} cos\theta & -sin\theta & 0 \\ sin\theta & cos\theta & 0 \\ 0 & 0 & 1 \end{pmatrix} \tag{8}$$

$$\mathbf{v} = \begin{pmatrix} \dot{x} \\ \dot{y} \\ 0 \end{pmatrix} \quad \boldsymbol{\Omega} = \begin{pmatrix} 0 \\ 0 \\ \omega \end{pmatrix} \tag{9}$$

The velocity of the sensors $\mathbf{S}_F$ and $\mathbf{S}_R$ can be derived by:

$$\dot{\mathbf{S}}_F = \mathbf{v} + T \cdot (\boldsymbol{\Omega} \times \mathbf{r}_f) = \begin{pmatrix} vcos\theta + \omega\frac{L_b}{2}cos\theta \\ vsin\theta + \omega\frac{L_b}{2}sin\theta \\ 0 \end{pmatrix} \tag{10}$$

$$\dot{\mathbf{S}}_R = \mathbf{v} + T \cdot (\boldsymbol{\Omega} \times \mathbf{r}_r) = \begin{pmatrix} vcos\theta + \omega\frac{L_b}{2}cos\theta + \omega L_a sin\theta \\ vsin\theta + \omega\frac{L_b}{2}sin\theta - \omega L_a cos\theta \\ 0 \end{pmatrix} \tag{11}$$

In this application, only the movement in lateral direction is considered. By referencing Eqs. (10) and (11) the dynamics of in lateral direction are expressed:

$$\dot{S_{Fy}} = vsin\theta + \omega\frac{L_b}{2}sin\theta \tag{12}$$

$$\dot{S_{Ry}} = vsin\theta + \omega\frac{L_b}{2}sin\theta - \omega L_a cos\theta \tag{13}$$

where S_{Fy} and S_{Ry} are the lateral components of $\mathbf{S}_F$ and $\mathbf{S}_R$. According to the geometric relations illustrated in Fig. 2, the guidance error of the machine at the reference point P can be expressed using S_f and S_r as:

$$e_\theta = \arctan\frac{S_r - S_f}{L_a} \tag{14}$$

$$e_y = e_S + sign(e_S)\frac{L_b}{2}(1 - cos\theta) \tag{15}$$

where $S_f = \|\mathbf{S}_F\|$ and $S_r = \|\mathbf{S}_R\|$, $e_S = S_f cos\theta - S_{ref}$ is the current lateral offset of the ultrasonic sensor SF, and S_{ref} is the desired side distance of the sensors SF and SR where $e_y = 0$ and $e_\theta = 0$.

The assignment of the time-optimal control is to find a control law of for transferring the system described by Eqs. (12) and (13) from an allowable initial state $(S_{Fy}(t_0),\ S_{Ry}(t_0))$ to the final state $(S_{Fy}(t_f) = S_{ref},\ S_{Ry}(t_f) = S_{ref})$ in minimum time with constraints in Eqs. (5) and (6). The cost function is to minimize the final time t_f:

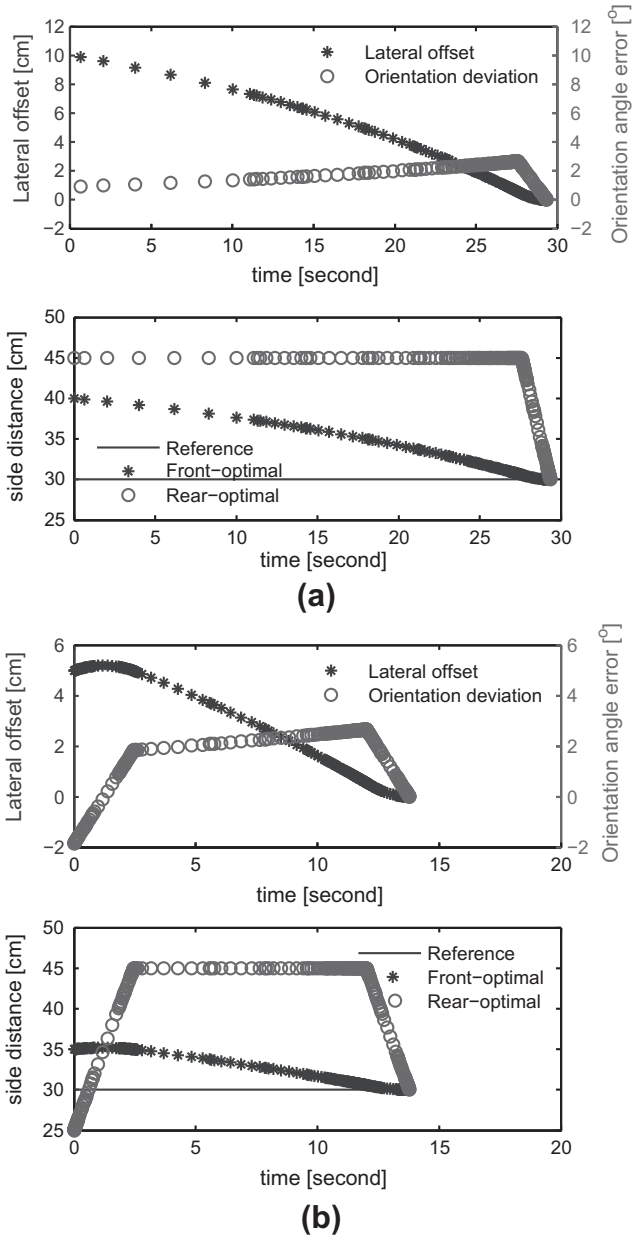

Fig. 3. Simulation results of minimum time-optimal control ((a) $S_{Fy}(t_0) = 40$ cm, $S_{Ry}(t_0) = 45$ cm; (b) $S_{Fy}(t_0) = 35$ cm, $S_{Ry}(t_0) = 25$ cm).

$$J = \int_{t_0}^{t_f} dt \tag{16}$$

The admissible control is constrained by:

$$|\omega| \leq 0.525\, rad/s \tag{17}$$

4.2. Simulation results

The minimum time problem described by equations from Eqs. (12)–(17) is solved using General Pseudospectral Optimization Software (GPOPS) (Rao et al., 2011), which is an open-source software of optimal control written in MATLAB environment. GPOPS implements the Gauss and Radau hp-adaptive pseudospectral collocation methods and has a build-in forward mode automatic differentiation and generates derivative estimates as efficiently as possible by adopting sparse finite-differencing of optimal control problem. The continuous-time optimal control problem is transcribed to a finite-dimensional nonlinear programming problem (NLP) that is solved using a restricted version of the NLP solver SNOPT (Gill et al., 2005).

The time-optimal control of row guidance system with constraints was solved using MATLAB. The forward velocity of the robot was set to 12 cm/s. The symmetries of the geometric trajectory was summarized by Balkcom and Mason (2000). Therefore, only the results of two representative cases were displayed in Fig. 3. For the first case, the machine started with an initial location of ($S_{Fy}(t_0) = 40$ cm, $S_{Ry}(t_0) = 45$ cm) for $e_y(t_0) > 0,\ e_\theta(t_0) > 0$, for the second case, the robot starts at ($S_{Fy}(t_0) = 35$ cm, $S_{Ry}(t_0) = 25$ cm) $e_y(t_0) > 0,\ e_\theta(t_0) < 0$.

For the first case, it is observed from the side distance plot that S_{Fy} declines continuously to the desired value S_{ref} , while S_{Ry} is kept at its upper bound before S_{Fy} approximates its desired value S_{ref}. Thereafter, S_{Ry} declines drastically to the desired value S_{ref}. The guidance error plot shows that the developing process of e_y is identical with that of S_{Fy}. The heading angle increases with the continuous reduction of S_{Fy} and a constant S_{Ry}, and decreases at the end of process with dramatic decline of S_{Ry}. For the second case in Fig. 3, the robot starts with $e_y(t_0) > 0$ while $e_\theta(t_0) < 0$, where e_y and e_θ are contrary in sign. It means that the robot faces an incorrect direction as it starts up. The side distance plot illustrates that S_{Ry} increases firstly to orientate the machine. S_{Fy} increases a bit at the beginning before S_{Ry} reaches S_{Fy}, which is named here orientation stage. After that, the developing tendency is the same as that by the first case. In the guidance error plot, e_θ is observed to rise rapidly at the first orientation stage. To sum up, all the initial errors were successfully eliminated and the system converged to the desired trajectory.

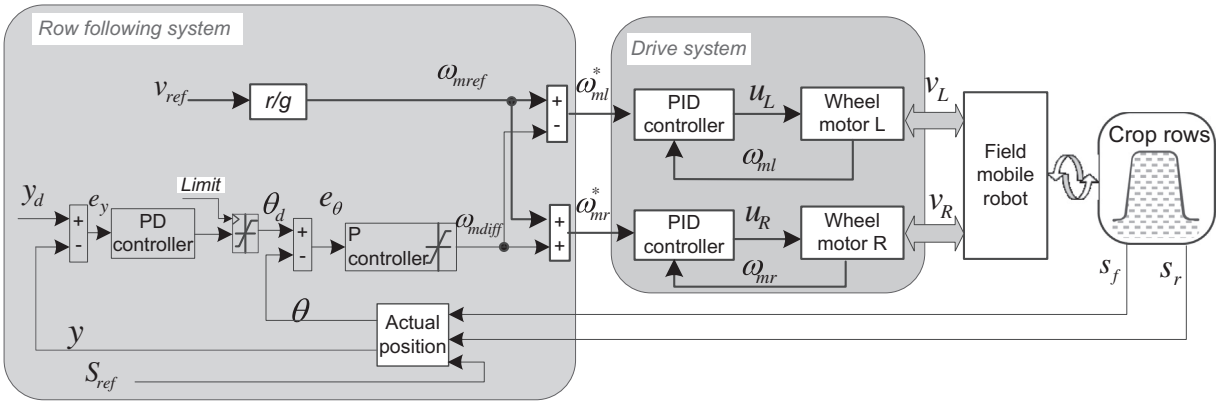

Fig. 4. Cascade substitute row guidance system for time-optimal control.

Table 1
Simulation and experimental parameters.

Parameter	Value
Wheel radius r (m)	0.3
Gear ratio g (–)	16 : 1
Vehicle width L_b (m)	2.1
Supply voltage $u(V)$	24
Motor inertia J_m (kg m^2)	0.0738
Motor inductance $L_m(H)$	1×10^{-4}
Viscous friction coefficient B_m (N m s rad^{-1})	4.3×10^{-3}
Back-emf constant K_e (V s rad^{-1})	0.45
Torque constant K_m (N m A^{-1})	0.45
Simplified gain motor closed-loop speed controller k_{ms} (–)	1
Simplified time constant motor closed-loop speed controller T_{ms} (s)	0.137
Proportional gain orientation controller $k_{p\theta}$ (s^{-1})	204
Proportional gain lateral controller k_{ky} (rad m^{-1})	10
Integral gain lateral controller k_{dy} (rad m^{-1})	3

From the simulation results, the rear side distance S_{Ry} of the time-optimal control solution was kept at its upper bound for $e_y(t_0) > 0$ wherever the robot starts up. As the robot and the drive motors are only permitted to drive forward, there are some infeasible initial positions which the robot cannot start with by this time-optimal process, such like ($S_{Fy}(t_0) = 40$ cm, $S_{Ry}(t_0) < 40$ cm), vice versa due to the spatial symmetry ($S_{Fy}(t_0) = 20$ cm, $S_{Ry}(t_0) > 20$ cm). For such infeasible positions, the signs of $e_y(t_0)$ and $e_\theta(t_0)$ are contrary, and $e_y(t_0)$ is at its upper or lower boundary. There is no region available for e_y at the upper boundary to rise and for e_y at the lower boundary to decrease at the orientation stage to correct the heading direction. Those infeasible positions should be avoided in the simulation studies of the time-optimal operations. This problem will be discussed and solved in the following practical design in Section 5.

5. Practical substitute system for time-optimal row guidance control

As discussed in Section 4, our guidance system is governed by a set of nonlinear state equations and furthermore the original time optimal control problem is subject to various constraints, such as initial and target conditions, state and control input constraints. Thus, it is difficult to get the analytical solution. As a result, the numerical solution method was used in this work. The well-developed optimal control software GPOPS, which integrates a third-party solver SNOPT. By using GPOPS, the original time-optimal control of the guidance system is converted into a large-scale constrained nonlinear programming problem. We note that implementation of such complex optimization algorithm in a typical low-cost hardware for our agricultural machine is unrealistic. This is because the available micro-controller system like PSoC 5 offers very limited memories and the clock frequency of the CPU is in the MHz range. All the aspects motivate us to explore computational cost-effective solutions. At the same time, we notice that there is a mapping of side distances (S_f, S_r) onto guidance error $(e_y,\ e_\theta)$ accordingly to Eqs. (14) and (15). Enlightened by the simulation results of the time-optimal control in Section 4, we seek an comparable solution by improving the cascade guidance system suggested in Dong et al. (2011).

The cascade controller consists of two-level structure shown in Fig. 4. Two independent speed loops at the low level are designed to stabilize the angular speeds of drive motors. A cascade structure, consisting of orientation inner loop and lateral offset outer loop, was adopted at the high level to get rid of the following deviation from the target row. As a prior try, the heading angle of the inner loop was simply constrained by setting a constant limitation to the output of lateral offset controller in the outer loop. For the cascade guidance system in Fig. 4, the forward velocity v_{ref} is preset. $\omega_{mref} = v_{ref}g/r$ is the equivalent angular speed of the drive motors with g the gear ratio and r radius of the drive wheel. ω_{mdiff} is the differential angular speed between the drive motors that is

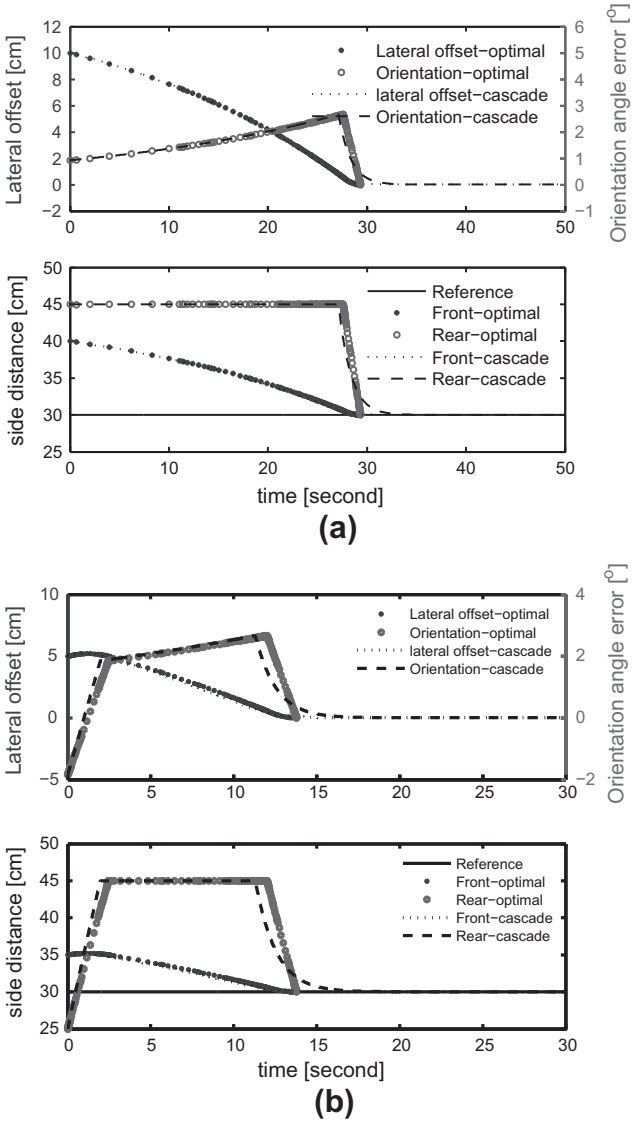

Fig. 5. Comparison simulation results ((a) $S_{Fy}(t_0) = 40$ cm, $S_{Ry}(t_0) = 45$ cm; (b) $S_{Fy}(t_0) = 35$ cm, $S_{Ry}(t_0) = 25$ cm).

given by the orientation angle controller. Here ω_{mdiff} is equivalent to the time-optimal control variable ω in Section 4. The desired angular speeds of the drive motors ω^*_{ml} and ω^*_{mr} are obtained through:

$$\omega^*_{ml} = \omega_{mref} - \frac{\omega_{mdiff}}{2} \tag{18}$$

$$\omega^*_{mr} = \omega_{mref} + \frac{\omega_{mdiff}}{2} \tag{19}$$

Differently from the time-optimal control discussed in Section 4, where the state variables are front and rear side distances S_{Fy} and S_{Ry}, the controlled variables of the substitute controller are e_y and e_θ. In order to prevent any collision between the field robot and cultivation beds, not only the lateral offset e_y, but also the heading angle of the machine e_θ must be efficiently constrained during operation. It is observed from the simulation results in Fig. 3 that there is no constant limitation to e_θ, which varies with the actual front side distance S_{Fy}. The lower and upper bounds of heading angle, θ^{lb} and θ^{ub}, can be accordingly expressed by:

$$\theta^{lb} = sign(e_S)\arctan\frac{S_r^{lb} - S_f}{L_a} \tag{20}$$

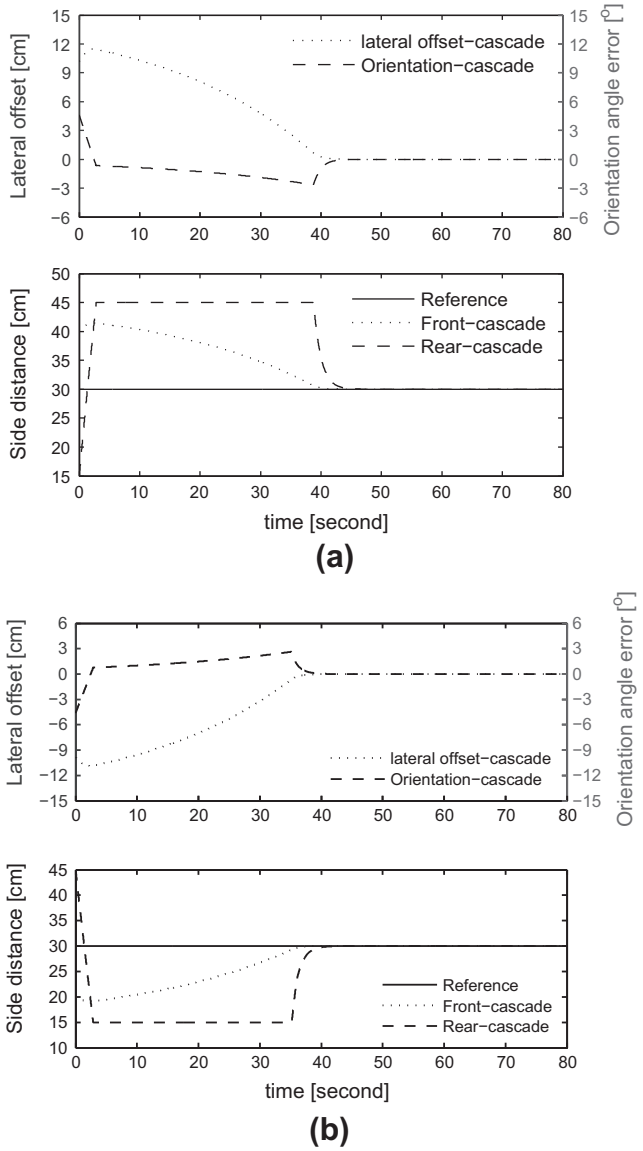

Fig. 6. Simulation results of critical situations ((a) $S_{Fy}(t_0) = 40$ cm, $S_{Ry}(t_0) = 15$ cm; (b) $S_{Fy}(t_0) = 20$ cm, $S_{Ry}(t_0) = 45$ cm).

$$\theta^{ub} = sign(e_S)\arctan\frac{S_r^{ub} - S_f}{L_a} \tag{21}$$

All the controllers including speed controllers of drive motors, lateral offset controller and orientation controller in this substitute system were designed using PID algorithms based on the kinematic model of the differential drive mobile robot. It was demonstrated in detail in Dong et al. (2011). The main parameters were given in Table 1.

5.1. Simulation results and discussion

To allow for a fair comparison between the substitute and the time-optimal controller, the same initial locations were applied. The comparison simulation results are shown in Fig. 5. It is illustrated that the simulation plots superpose with each other quite well. The only minor difference between the two systems is the development of S_{Ry} from its upper bound to the desired value. It is also observed by e_θ. It can be easily explained with the cascade control structure. Differently from the numerical solution of time-optimal control, the outer loop of the cascade controller is kept saturated to allow the lateral offset e_y to fall as soon as possible. e_θ begins to fall only when the outer loop of lateral offset retreats from saturation.

As discussed in Section 4, for the time-optimal design the machine cannot start up from such initial locations as ($S_{Fy}(t_0) =$ 40 cm, $S_{Ry}(t_0) < 40$ cm) or ($S_{Fy}(t_0) = 20$ cm, $S_{Ry}(t_0) > 20$ cm)

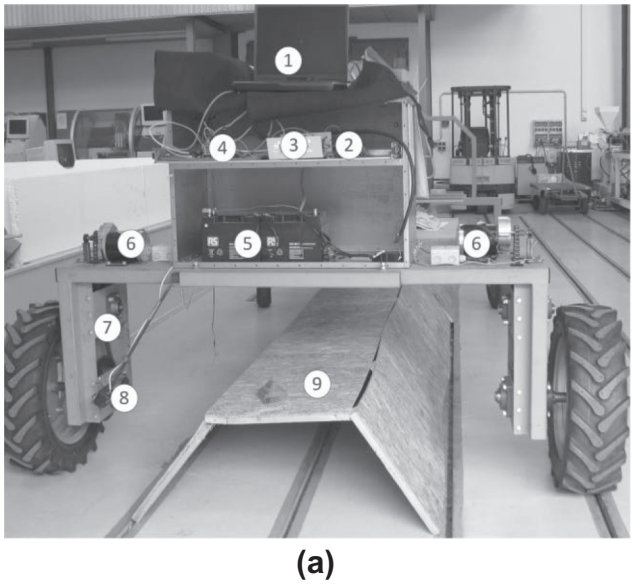

Fig. 7. Experimental platform ((a) Setup: 1. Laptop, 2. Joystick, 3. Sabertooth, 4. PSoC processor, 5. Battery, 6. DC motor, 7. Chain gear box, 8. Ultrasonic sensor, 9. Model of cultivation bed; (b) schematic illustration of row guidance control system).

because the constraint on S_{Fy} must be tightly held in solving the time-optimal control problem. This problem was solved in the cascade substitute system. The simulation results with two critical initial positions, where $S_{Fy}(t_0) = 40$ cm, $S_{Ry}(t_0) = 15$ cm and $S_{Fy}(t_0) = 20$ cm, $S_{Ry}(t_0) = 45$ cm, were shown in Fig. 6. In Fig. 6(a) to get rid of the initial errors the robot is required to orientate itself firstly, which causes increase in front side distance and results in exceeding the soft constraints imposed on S_{Fy} by 2 cm. The plots in Fig. 6(b) show the symmetrical results. It is completely acceptable according to the original constraints $S_{ref} \pm 15$ cm.

It is concluded that the improved substitute controller fulfill the guidance objective of the time-optimal system successfully by properly setting constraints to the desired heading angle. The controller based on PID method economizes expensive computation costs. Moreover, the startup problem with critical initial positions was also solved with the cascade guidance system. Therefore, the substitute design is preferable and practical to be implemented on micro-processor. Consequently, we put only the cascade substitute system in practice on the experimental platform.

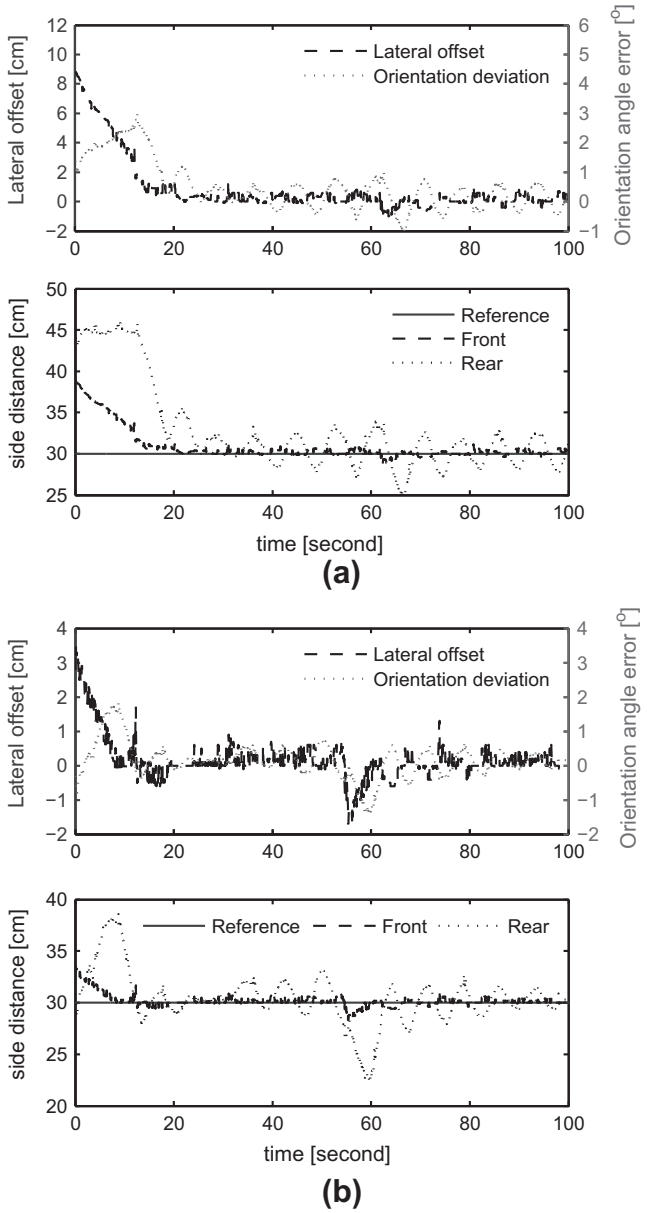

Fig. 8. Experimental results in laboratory ((a) $S_{Fy}(t_0) = 38.8$ cm, $S_{Ry}(t_0) = 44$ cm; (b) $S_{Fy}(t_0) = 33.5$ cm, $S_{Ry}(t_0) = 28$ cm).

5.2. Experimental results in laboratory

The experimental setup were shown in Fig. 7. The control loops at low level were performed with a frequency of 200 Hz. The cascade system at the high level worked with a frequency of 20 Hz. The forward linear velocity of the machine is set to 12 cm/s. The processing data were saved on a computer through USB cable. The guidance performance was investigated against varied initial positions and lateral offset. Each experiment was executed repeatedly, and the similar results were achieved. The two representative experimental results were illustrated in Fig. 8.

For the first study, the robot started with an initial position of ($S_{Fy}(t_0) = 38.8$ cm, $S_{Ry}(t_0) = 44$ cm), which is comparable with the simulation case in Fig. 5. To evaluate the guidance performance against external disturbance, a lateral offset of about 1.5 cm was introduced at about $t = 60$ s. The experimental results coincided quite well with the simulation results in Fig. 5. The converging process of this experimental case is about 10 s shorter than the simulation results of the first case study in Fig. 5 due to the smaller initial lateral offset. Fig. 8(b) shows the experimental results where the robot started with ($S_{Fy}(t_0) = 33.5$ cm, $S_{Ry}(t_0) = 28$ cm). S_{Fy} converges to the desired value before S_{Ry} reaches its upper bound. In both cases, the experimental results coincide closely with those of the numerical studies. The only difference of the experimental results from the numerical ones is that S_{Ry} (or e_θ) fluctuates continuously around its desired value in that e_y is not strictly kept at its desired value in the experimental tests, and the adjustment of the following error is only realized by modifying S_{Ry} (or e_θ). Altogether, all the initial error and the introduced disturbance were successfully eliminated with the proposed practical guidance system. A following precision of ± 0.5 cm for the reference point P of the robot was achieved.

5.3. Verification in field

The field robot with the proposed cascade row guidance strategy was put in real cultivation field of white asparagus to investigate the following operation under the situations (see Fig. 9). The experiments were carried out at later season of white asparagus. The cultivation bed was considerably out of shape with time lapse and weeds. The sandy ground surface was rather soft due to drought. The test results are illustrated in Fig. 10. The forward velocity varied from minimal 12 cm/s (see Fig. 10(a)) to maximal 50 cm/s with a load of 80 kg (Fig. 10(b)). The measuring noise was caused by roughness of the sandy and weedy side surface of the cultivation bed. The initial errors were efficiently compensated with the practical substitute controller. The robot succeeds in

Fig. 9. On-site investigation in field.

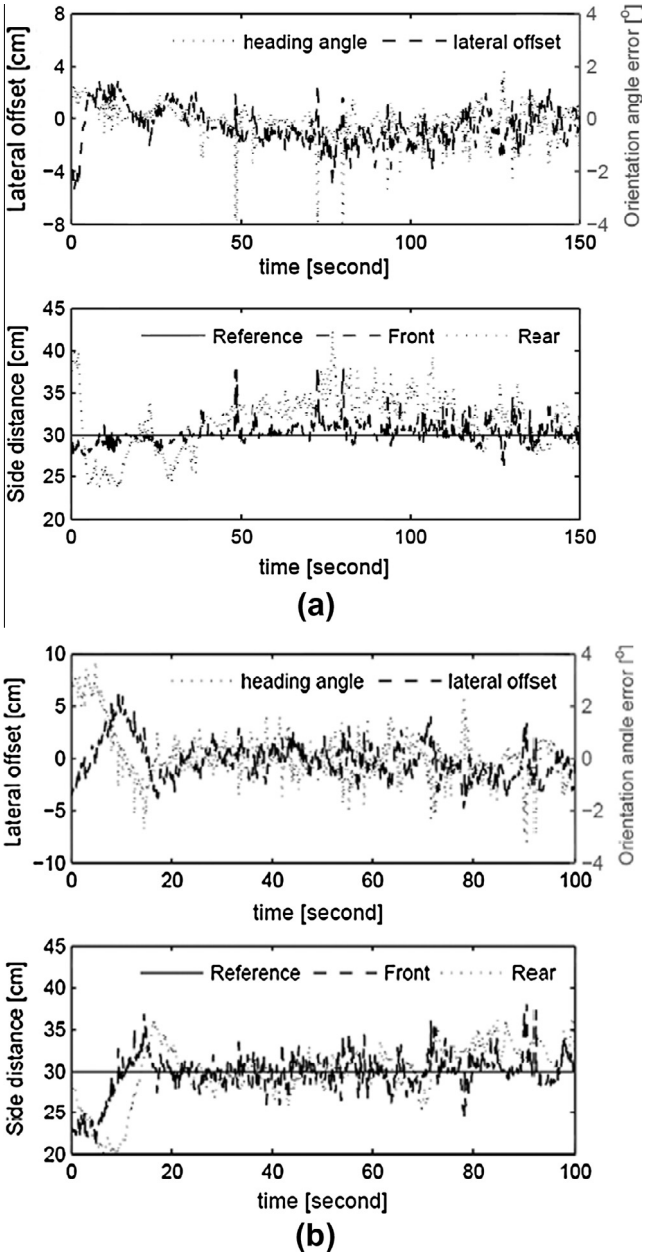

Fig. 10. Experimental results in field ((a) $S_{Fy}(t_0) = 28$ cm, $S_{Ry}(t_0) = 40$ cm, $v_{ref} = 12$ cm/s; (b) $S_{Fy}(t_0) = 22.7$ cm, $S_{Ry}(t_0) = 27.8$ cm, $v_{ref} = 50$ cm/s).

driving along the target row against external disturbance in field. It is shown that the practical row guidance system works quite well and a following precision of roughly ± 3 cm for e_y has been achieved under the on-site situations.

6. Conclusion

Under consideration of the cultivation features, the time-optimal guidance control problem has been formulated based on the kinematics model of the differential drive wheeled mobile robot. The intra-row position was expressed using the front and rear distances measured by ultrasonic sensors. Subsequently, the time-optimal control problem was numerically solved using the open source optimal control software GPOPS. Based on the analysis of the numerical results of the time-optimal control, a cascade controller based on PID method was improved as a practical substitute to perform time-optimal control performance. By properly adjusting the constraints to the heading angle in the inner loop of cascade controller at the high level, the substitute successfully accomplished the tasks of the time-optimal control. Since the substitute was designed based PID algorithm, the complex nonlinear optimization problem that is essential in solving time-optimal control program was avoided. The practical cascade system not only improves the computing efficiency in the simulation studies, but also allows for an effortless implementation on the PSoC 5 based hardware platform. The efficiency of the proposed row guidance strategy has been thoroughly investigated. A satisfying guidance performance with a precision of ± 3 cm has been achieved in the field test.

Our future work will focus upon integration of the platform with cascade row guidance system with the harvesting apparatus, aiming at constructing a prototype of an autonomous machine for white asparagus harvesting. With more investment an autonomous navigation guidance with help of RTK GPS for the harvesting robot would be further investigated.

References

Åstrand, B., Baerveldt, A.J., 2002. An agricultural mobile robot with vision-based perception for mechanical weed control. Autonomous Robots 13, 21–35.

Bakker, T., van Asselt, C.J., Bontsema, J., Mller, J., van Straten, G., 2004. A vision based row detection system for sugar beet. In: Computer-Bildanalyse in der Landwirtschaft Workshop, Potsdam-Bornim/Braunschweig, Germany, vol. 37, p. 42C55.

Bakker, T., van Asselt, C.J., Bontsema, J., Mller, J., van Straten, G., 2011. Autonomous navigation using a robot platform in a sugar beet field. Biosystems Engineering 109 (4), 357–368.

Balkcom, D.J., Mason, M.T., 2000. Geometric construction of time optimal trajectories for differential drive robots. In: Proceedings of the Fourth Workshop on the Algorithmic Foundations of Robotics (WAFR), pp. 1–13.

Chatzimichali, A.P., Georgilasand, I.P.V., Tourassis, D., 2009. Design of an advanced prototype robot for white asparagus harvesting. In: Proceedings of IEEE/ASME International Conference on Industrial Advanced Intelligent Mechatronics, Singapore, 14–17 July.

Díaz del Río, F., Jiménez, G., Sevillano, J.L., Vicente, S., Civit Balcell, A., 2001. A path following control for unicycle robots. Journal of Robotic Systems 18 (7), 325–342.

Dong, F., Heinemann, W., Kasper, R., 2011. Development of a row guidance system for an autonomous robot for white asparagus harvesting. Computers and Electronics in Agriculture 79, 216–225.

Feng, L., Koren, Y., Borenstein, J., 1993. Cross-coupling motion controller for mobile robots. IEEE Transactions on Control Systems 13 (6), 35–43.

Gill, P.E., Murray, W., Saunders, M.A., 2005. SNOPT: an SQP algorithm for large-scale constrained optimization. Society for Industrial and Applied Mathematics 47 (1), 99–131.

Gracia, L., Tornero, J., 2008. Kinematic control of wheeled mobile robots. Latin American Applied Research 38, 7–16.

Mehta, S.S., Burks, T.F., Dixon, W.E., 2008. Vision-based localization of a wheeled mobile robot for greenhouse applications: a daisy-chaining approach. Computers and Electronics in Agriculture 63, 28–37.

Rao, A.R., Benson, D., Darby, C.L., Huntington, G.T., 2011. User's manual for GPOPS version 4.x: A MATLAB software for solving multiple-phase optimal control problem using hp-adaptive pseudospectral methods.

Sànchez-Hermosilla, J., Rodrìguez, F., Gonzàlez, R., Guzmàn, J.L., Berenguel, M., 2010. A mechatronic description of an autonomous mobile robot for agricultural tasks in greenhouses. *Mobile Robots Navigation*, pp. 583–608.

Slaughter, D.C., Giles, D.K., Downey, D., 2008. Autonomous robotic weed control systems: a review. Computers and Electronics in Agriculture 61, 63–78.

Tanigaki, K., Fujiura, T., Akase, A., Imagawa, J., 2008. Cherry-harvesting robot. Computers and Electronics in Agriculture 63, 65–72.

Van Henten, E.J., Hemming, J., Van Tuijl, B.A.J., Kornet, J.G., Bontsema, J., 2003. Collision-free motion planning for a cucumber picking robot. Biosystems Engineering 63, 583–608.

Xue, J., Zhang, L., Grift, T.E., 2012. Variable field-of-view machine vision based row guidance of an agricultural robot. Computers and Electronics in Agriculture 84, 85–91.